High-resolution far ultraviolet spectrum of electron-excited SO_2

Prahlad Vatti Palle and Joseph Ajello
Jet Propulsion Laboratory, California Institute of Technology, Pasadena, California, USA

Anil Bhardwaj
Space Physics Laboratory, Vikram Sarabhai Space Centre, Trivandrum, India

Received 7 January 2003; revised 2 October 2003; accepted 10 November 2003; published 26 February 2004.

[1] The high-resolution UV capabilities ($\lambda/\Delta\lambda = 10^5$) of the Hubble Space Telescope (HST) equipped with the Space Telescope Imaging Spectrograph (STIS) reflects a need for a high-resolution laboratory UV spectral data base for comparison with observation. For the purpose of interpreting the astronomical observations of Io by HST the electron-excited UV spectrum of SO_2 gas has been studied from 800–1700 Å at medium ($\lambda/\Delta\lambda \sim 10^3$) and high resolution ($\lambda/\Delta\lambda \sim 5 \times 10^4$) . The far ultraviolet (FUV) laboratory spectrum consists entirely of S I, II and O I, II multiplets. From a measurement of the medium resolution spectrum at 1.5 Å FWHM we are able to provide new detail in the 200 eV emission cross sections for all the FUV features. At 30 and 100 eV electron-impact energy we have measured high resolution emission spectra of the fine structure lines of the atomic multiplets at 1256 Å from S II, at 1304 Å from O I, 1479 Å from S I and at 1429 Å from S I at 100 eV electron-impact energy. At 100 eV electron-impact energy we compare the optically thin laboratory spectrum of the atomic multiplet S I at 1479 Å with the model spectrum of electron excitation of atomic sulfur. In addition, we compare a HST STIS observation of Io with the G140M grating (FWHM $\sim$ 0.5 Å) at 1479 Å with a laboratory spectrum after transmission through a layer of atomic S. We have also compared our laboratory spectrum to FUV observations by STIS reported by *Roesler et al.* [1999]. The relative intensities of the strongest lines of S I and O I are compared with the laboratory emission cross sections for SO_2 near 40 eV (3 Ryd) electron energy. The Doppler line profiles of individual fine structure lines of atomic sulfur and oxygen were used to ascertain the kinetic energy distribution from dissociative excitation at 30 and 100 eV. At 100 eV electron-impact energy we find the kinetic energy distribution of the oxygen and sulfur atoms to be in the range of 2 eV to 3 eV. At 30 eV electron-impact energy we place an upper limit on the kinetic energy of sulfur and oxygen atoms as <1 eV. We provide the first measurement of the O I] 1356 Å absolute excitation function and the estimate of the cross section ratio O I] 1356 Å/1304 Å as a function of energy. We establish the absolute cross section of O I 1304 Å as $2.3 \pm 0.5 \times 10^{-18}$ cm^2 at 100 eV and the estimated cross section of O I] 1356 Å as $2.1 \pm 1 \times 10^{-18}$ cm^2 at 100 eV. *INDEX TERMS:* 6218 Planetology: Solar System Objects: Jovian satellites; 0310 Atmospheric Composition and Structure: Airglow and aurora; 6026 Planetology: Comets and Small Bodies: Ionospheres—composition and chemistry; 6005 Planetology: Comets and Small Bodies: Atmospheres—composition and chemistry; 6060 Planetology: Comets and Small Bodies: Radiation and spectra; *KEYWORDS:* Jovian satellites, airglow aurora, electron impact, ultraviolet emissions

Citation: Vatti Palle, P., J. Ajello, and A. Bhardwaj (2004), High-resolution far ultraviolet spectrum of electron-excited SO_2, *J. Geophys. Res.*, *109*, A02310, doi:10.1029/2003JA009828.

1. Introduction

[2] Details of Io's extended atmosphere and of the neutral molecular and atomic gases surrounding the satellite are becoming available with spectroscopic images, in the UV from STIS [*Roesler et al.*, 1999; *Wolven et al.*, 2001] and visible photometric images from Galileo Solid State Imaging (SSI) system and Cassini imaging subsystem (ISS) (P. E. Geissler, private communication, 2003) obtained while in eclipse [*Geissler et al.*, 1999]. The plasma and torus consisting of ionized sulfur and oxygen while corotating with Jupiter deposits its energy in the upper atmosphere by heating, ionizing, and dissociating the SO_2 parent gas in a quasi-steady state regime maintaining the upper atmosphere distribution of sulfur and oxygen atoms [*Wong and Smyth*, 2000]. Both direct torus electrons and secondary electrons are especially reactive in collision processes

0148-0227/04/2003JA009828$09.00

because the excitation cross sections of the atmospheric gases, as well as the electron-impact energy distribution produced in the ionosphere, attain their peak values at low energies, typically from a few tenths of an eV to about 100 eV.

[3] The bright O I 1304 Å and O I] 1356 Å emission lines observed by HST from Europa and Ganymede [*Hall et al.*, 1995, 1998; *Feldman et al.*, 2000], the intense UV emission from the Io plasma torus observed by Galileo and Cassini [*Esposito et al.*, 2003], and the intense O I 1304 Å and O I] 1356 Å line emissions dominating the recent FUV spectra of the Io equatorial hotspots obtained near western elongation [*Frank et al.*, 1996; *Roesler et al.*, 1999; *Retherford et al.*, 2000], all clearly demonstrate the importance of the electron-impact-induced excitation and subsequent fluorescence from atomic and molecular species, together with their ions such as O, S, SO_2, SO, O^+, S^+, O^{++}, S^{++}, and SO_2^{++} [*Michael and Bhardwaj*, 2000]. The auroral FUV spectrum of Io is more complicated than the spectra from Europa or Ganymede with many bright S I and S II emission features [*Feaga et al.*, 2002; *Clarke et al.*, 1994]. A fundamental limitation in measuring the compositional structure and the energy deposition is set by the accuracy of the emission cross sections used in energy-loss codes [*Bhardwaj and Michael*, 1999b], as well as the identity of the parent oxygen-bearing species, i.e., O, O_2, SO_2, SO, etc., responsible for the observed emissions at 1304 and 1356 Å [*Bhardwaj and Michael*, 1999a]. In the recent review of Io's extended atmosphere, *Spencer and Schneider* [1996] pointed out that the utility of FUV observations of neutral O and S emissions are hampered by an inadequate atomic physics database.

[4] We have undertaken a laboratory spectroscopic study of electron-excited SO_2 in a single-scattering, optically thin experiment to build on the cross sections studies reported in our earlier work at low resolution [*Ajello et al.*, 1992a, 1992b]. The work described herein provides new cross section data by which astronomers will be able to accurately model the observed intensities within the atmosphere of Io for the portion of the atomic sulfur and oxygen line multiplet emission spectrum caused by electron impact dissociative excitation of SO_2, the dominant gas in the atmosphere of Io. We also study for the first time the fine structure intensities of the strongest atomic oxygen and sulfur multiplets found in the FUV at S II 1256 Å, O I 1304 Å, S I 1429 Å and S I 1479 Å. We compare the structure to that observed by the G140M grating (FWHM $\sim$ 0.5 Å) with the wide slit (2″ aperture) of STIS and GHRS. Based on our knowledge of an HST archive search the only medium resolution studies of the atomic multiplets in the UV were obtained for S II 1256 Å, S I 1479 Å and O I] 1356 Å. We will compare, where possible, our laboratory spectra of S and O multiplets at high resolution to HST STIS and GHRS spectra. The comparison may help to confirm or discount SO_2 as a major source for direct excitation of the atomic multiplets. We will also estimate the amount of atomic self-absorption by atomic S in the S I 1479 Å multiplet as *Feaga et al.* [2002] have done for the case of direct excitation of atomic S.

[5] If SO_2 dissociation contributes to the UV emission of Io, electrons with energies 30 eV or more would be required, so any measurable contribution is strong evidence of super-thermal electrons (energy >30 eV) impacting Io's upper atmosphere. Recent high-resolution ground-based studies of the line profile of the O I 6300 Å optically forbidden red line by *Oliversen et al.* [2001] indicates a rapidly varying broad line width (FWHM $\sim$ 0.1 Å). The broad FWHM correlates with intensity. The fluctuating broad line width, which can be greater than instrumental spectral resolution (0.05 Å) indicates that molecular dissociation contributes to the visible line emissions. A plausible reason for the fluctuations is a time variable energy flux component of field-aligned nonthermal ($\sim$30 eV) electrons found in the Galileo Plasma Analyzer (PLS) data in the vicinity of Io and the Io torus [*Frank and Paterson*, 1999, 2000; *Oliversen et al.*, 2001]. These electrons are referred to as the nonthermal "tail" of the electron distribution. Both the thermal "cold ($\sim$4–5 eV)" and the nonthermal "tail" electron distributions were observed by the Galileo PLS [*Frank and Paterson*, 1999, 2002; cf. *Oliversen et al.*, 2001]. In this laboratory study we find similar magnitudes for line widths of atomic species in the FUV from dissociative excitation of SO_2.

[6] In this paper we present the combined EUV and FUV spectra (800–1700 Å) of electron-impact induced fluorescence from SO_2 at a medium resolution of 1.5 Å and 200 eV electron-impact energy. The spectral identifications and the cross sections reported here (Table 1) represent a marked improvement over our earlier work performed at 5eÅ resolution [*Ajello et al.*, 1992a, 1992b]. We describe here our laboratory procedure for determining the emission cross section for the atomic multiplet at O I 1304 Å from SO_2 at 100 eV electron-impact energy, which we use throughout this work as the "bench-mark" for estimating emission cross sections for all the identified spectral features. We chose to study at high resolution (95 mÅ) the spectra of the strongest atomic multiplets observed at Io. We present here the high-resolution spectra of these atomic multiplets: S II 1256 Å, O I 1304 Å, S I 1429 Å, and S I 1479 Å at 100 eV electron-impact energy and also for O I 1304 Å and S I 1479 Å at 30 eV electron-impact energy. We present here an extension of the technique developed previously [*Makarov et al.*, 2003; *Kanik et al.*, 2003] in our laboratory for determining the cross section of the optically forbidden O I] 1356 Å emission produced from O_2 to report our preliminary estimate of the cross section for O I] 1356 Å emission produced from SO_2 at 100 eV electron-impact energy. We also describe the analysis of our measurements of relative excitation functions for O I 1304 Å ($^3P \leftarrow {}^3S^0$) and O I] 1356 Å ($^3P \leftarrow {}^5S^0$) transitions to determine the cross section ratio, O I 1304 Å/O I] 1356 Å, as a function of energy for a monoenergetic distribution of electrons.

[7] The high-resolution 3-m laboratory UV spectrometer was employed for the measurements of the Doppler profiles of atomic S and O multiplets and their ions from dissociative excitation. In this paper we present Doppler line profiles of O I 1302.168 Å, O I 1152.151 Å, S I 1473.994 Å and S I 910.485 Å fine structure lines. A study of the two multiplets at S I 1479 Å ($^3P \leftarrow {}^{3,5}D^0$) are similarly interesting. They are composed of dipole allowed fine structure lines and optically forbidden intercombination

Table 1. Features of Dissociative Emission Spectrum of SO_2 From 850 to 1700 (See Figure 1) Upon Electron Impact at 200 eV[a]

Feature	Integrated Wavelength Interval (Å)	Species	Wavelength (Å)	Cross section (10^{-18} cm^2) Present Study	*Ajello et al.* [1992]
1	871.000–887.000			0.19	0.19
1a	871.000–878.000	S II	875.415	0.095	
		S II	875.650		
		S II	877.675		
		O I	877.201		
		O I	877.798		
		O I	877.879		
1b	878.000–887.000	O I	878.9728	0.095	
		O I	879.019		
		O I	879.100		
		O I	79.551		
		S II	881.359		
		O I	882.890		
2	887.000–900.000			0.093	0.11
2a	887.000–894.000	S II	894.426	0.074	
2b	894.000–900.000	S II	894.799	0.019	
3	900.000–925.400			0.666	0.54
3a	900.000–905.600	S III	900.242	0.023	
			901.668		
			902.561		
3b	905.600–909.400	S II	906.870	0.028	
3c	909.400–912.600	S II	910.490	0.179	
3d	912.600–914.800	S II	912.740	0.096	
3e	914.800–918.400	S II	915.390	0.040	
3f	918.400–921.000	S II	918.820	0.027	
			919.240		
3g	921.000–925.000	O I	922.008	0.024	
		O I	922.073		
		O I	929.517		
4	925.400–944.000			0.37	0.28
4a	925.000–928.000	O I	924.950	0.022	
		O I	926.306		
		O I	926.896		
4b	928.000–934.000	O I	930.257	0.038	
		O I	930.886		
		O I	931.482		
		O I	931.628		
		O I	932.225		
4c	934.000–944.000	O I	935.193	0.31	
		O I	936.630		
		S II	937.410		
		S II	937.841		
		O I	937.630		
		O I	938.020		
		O I	938.625		
		O I	939.235		
		O I	939.841		
5	944.000–954.000	O I	948.686	0.084	0.087
		O I	950.112		
		O I	950.733		
		O I	950.885		
		O I	952.318		
		O I	952.841		
6	954.000–965.000	S II	957.880	0.034	0.065
7	965.000–983.000			0.215	0.2
7a	965.000–975.800	S II	968.370	0.170	
		O I	971.738		
		O I	973.234		
		O I	973.885		
		O I	976.448		
7b	975.800–983.000	O I	977.959	0.045	
		O I	978.617		
8	983.000–998.000			1.06	0.66
8a	983.000–994.000	O I	988.578	0.84	
		O I	988.655		
		O I	988.773		
		O I	990.127		
		O I	990.204		
		O I	990.801		
8b	994.000–998.000	S II	996.000	0.22	
9	998.000–1004.00	O I	999.497	0.23	0.21
		S II	100.048		
		S II	100.075		
10	1004.00–1012.00	S II	100.615	0.24	0.17
			100.695		
11	1012.00–1019.00	S III	101.249	0.17	0.11
		S II	101.409		
		S II	101.442		
		S III	101.551		
12	1019.00–1036.00			0.70	0.47
12a	1019.00–1024.00	S II	1019.530	0.104	
		S III	1021.100		
		S III	1021.320		
		S II	1021.539		
12b	1024.00–1030.40	O I	1025.762	0.554	
		O I	1027.431		
		O I	1028.157		
		S II	1030.870		
12c	1030.40–1036.00	S II	1031.340	0.042	
13	1036.00–1053.00			0.366	0.31
13a	1036.00–1044.00	O I	1039.230	0.190	
		O I	1040.943		
		O I	1041.688		
13b	1044.00–1053.00	S II	1045.740	0.176	
		S II	1047.560		
		S II	1047.860		
		S II	1048.430		
		S II	1049.060		
		S II	1050.283		
		S II	1053.210		
14	1074.00–1088.00				
14a	1074.00–1083.00	O II	2 × (538.256)		
		O II	2 × (538.318)		
		O II	2 × (539.086)		
		O II	2 × (539.547)		
14b	1083.00–1088.00	O II	1083.134	0.019	
		O II	1085.052		
		O II	1086.024		
15	1091.00–1109.00			0.29	0.17
15a	1091.00–1100.00	S II	1096.570	0.097	
15b	1100.00–1109.00	S II	1101.975	0.193	
		S II	1102.320		
16	1122.00–1137.00			0.088	0.084
16a	1122.00–1128.00	S II	1124.390	0.053	
		S II	1124.978		
		S II	1125.000		
16b	1128.00–1137.00	S II	1131.052	0.035	
		S II	1131.658		
17a	1147.00–1160.00	O I	1152.151	0.453	0.25
17b	1189.80–1192.40	S I	2 × (594.470)		
17c	1193.40–1196.40	S I	2 × (597.497)		
		S I	2 × (597.758)		
18	1200.00–1210.00			0.798	0.64
20b	1230.00–1238.00	S I	1231.300	0.065	
		S I	1233.600		
		S I	1233.922		
		S I	1234.140		
		S I	1235.624		
		S I	1236.632		
		S I	1238.340		
21	1247.00–1268.00			1.063	1.0

Table 1. (continued)

Feature	Integrated Wavelength Interval (Å)	Species	Wavelength (Å)	Cross section (10^{-18} cm^2) Present Study	*Ajello et al.* [1992]
21a	1247.00–1249.40	S I	1247.160	0.0162	
		S I	1248.044		
21b	1249.40–1252.80	S II	1250.500	0.166	
		S I	1250.814		
21c	1252.80–1257.00	S I	1253.297	0.329	
		S I	1253.970		
21d	1257.00–1262.40	S I	1259.530	0.540	
21e	1262.40–1268.00	S I	1262.859	0.120	
22	1269.00–1277.00	S I	1269.028	0.048	0.07
		S II	1207.270		
		S I	1270.782		
		S II	1271.555		
		S I	1272.075		
		S II	1276.132		
23	1276.00–1285.00			0.08	0.062
23a	1276.00–1279.40	S I	1277.199	0.05	
		S I	1277.216		
		S II	1277.450		
		S II	1279.028		
23b	1279.40–1285.00	S II	1279.489	0.03	
		S I	1280.991		
		S II	1283.350		
		S II	1284.962		
24	1294.00–1314.00			1.719	1.54
24a	1294.00–1299.00	S I	1296.174	0.0750	
24b	1299.00–1304.00	O I	1302.117	0.904	
		S I	1302.337		
		S I	1302.863		
		S I	1303.110		
		S I	1303.429		
24c	1304.40–1314.00	O I	1304.857	0.74	
		S I	1305.883		
		O I	1306.029		
		S I	1301.940		
		S I	1313.249		
25a and 25b	1314.00–1327.00			0.19	0.212
25a	1314.00–1321.00	S I	1316.542	0.11	
		S I	1316.618		
25b	1321.00–1327.00	S I	1323.153	0.08	
		S I	1323.522		
		S I	1326.643		
25c	1327.00–1328.20	S II	2 × (664.314)	0.013	
25d	1329.20–1330.60	S II	2 × (665.520)		
25e	1334.00–1337.80	S II	2 × (669.107)		
26a and 26b	1354.00–1368.00			0.06	0.083
26a	1354.00–1358.00	O I	1355.598	1.87	
		O I	1358.512		
26b	1358.00–1368.00	S II	1363.011	0.047	
		S II	1363.384		
26c	1374.00–1375.80	S II	2 × (687.551)		
		S II	2 × (687.776)		
		S II	2 × (687.992)		
27	1381.00–1416.00			0.307	0.354
27a	1381.00–1384.00	S I	1381.552	0.032	
27b	1384.00–1387.60	S I	1385.041	0.021	
		S I	1385.510		
27c	1387.60–1391.00	S I	1388.435	0.070	
		S I	1389.154		
27d	1391.00–1395.00	S I	1392588	0.028	
27e	1395.00–1400.00	S I	1396.112	0.055	
27f	1400.00–1405.00	S I	1401.514	0.049	
27g	1405.00–1412.00	S I	1409.337	0.037	
27h	1412.00–1416.00	S I	1412.873	0.015	
		S I	1414.265		
28	1419.00–1430.00	S I	1425.030	0.359	0.368
		S I	1425.188		
		S I	1425.219		
29	1430.00–1443.00			0.328	0.351
29a	1430.00–1435.80	S I	1432.800	0.229	
		S I	1433.105		
29b	1435.80–1443.00	S I	1436.963	0.099	
30a	1443.00–1451.00	S I	1442.967	0.046	0.048
		S I	1448.229		
30b	1458.60–1460.20	S II	2 × (729.788)		
30c	1463.00–1465.20	S II	2 × (732.435)		
31	1469.00–1481.00	S I	1471.832	0.805	0.738
		S I	1472.503		
		S I	1472.972		
		S I	1473.019		
		S I	1473.995		
		S I	1473.800		
		S I	1475.472		
32	1481.00–1492.00			0.544	0.504
32a	1481.00–1485.40	S I	1481.665	0.418	
		S I	1481.712		
		S I	1483.039		
		S I	1483.233		
32b	1485.40–1492.00	S I	1485.622	0.126	
		S I	1487.150		
33a	1528.40–1533.20	S II	2 × (763.656)		
		S II	2 × (764.416)		
		S II	2 × (765.387)		
		S II	2 × (765.478)		
		S II	2 × (765.574)		
		S II	2 × (765.684)		
33b	1560.00–1564.00	O II	1560.094	0.052	
		O II	1562.989		
		O II	1563.511		
		O II	1563.708		
33c	1615.00–1621.00	O II	1616.929	0.052	
		O II	1617.756		
		O II	1619.321		
33d	1655.00–1662.00	O II	1653.545	0.091	
		O II	1654.868		
		O II	1655.517		
		O II	1657.392		
33e	1662.00–1678.00	S II	1664.880	0.402	0.371
		S II	1666.687		
		S II	1667.089		
34	1683.00–1690.00	S I	1687.531	0.031	0.03

[a]Features 1–17a, 18–25a, 26a, 27–30a, 31, 32, 33e, and 34 have been identified by *Ajello et al.*, 1992. For second order features indicated as 2X in wavelength, the cross sections could not be estimated. The values given here up to four significant figures serve to indicate the relative magnitudes of the various features. They do not represent the accuracy of the individual one.

lines. We compare the laboratory measured fine structure of the S I 1479 Å multiplet at 0.09 Å resolution from electron-excited SO_2 with a model of electron-excited sulfur [*Zatsarinny and Tayal*, 2002]. We conclude this paper with a discussion of application of these high-resolution studies to STIS and GHRS observations of Io. Specifically, for the S I 1479 Å multiplets we compare the recent STIS observation using the G140M grating presented in *Feaga et al.* [2002] with a laboratory model based on electron-impact excitation of SO_2.

2. Medium Resolution Spectrum

[8] The experimental apparatus and vacuum ultraviolet (VUV) calibration techniques have been described earlier in

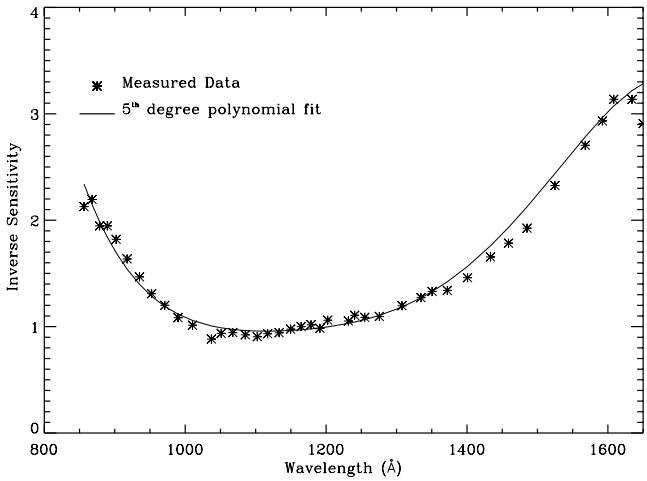

Figure 1. Inverse sensitivity curve for the experimental set-up wavelength range 850–1700 Å. A fifth degree polynomial could be fitted through the data. The fitted data was used to calibrate (relative calibration) the intensities of the measured spectra.

detail [*Liu et al.*, 1995; *Ajello et al.*, 1996]. In brief, the apparatus consists of an electron impact collision chamber in tandem with a high resolution ($\lambda/\lambda\Delta$ = 5000) Acton 3.0 m VUV spectrometer. The emitted photons were detected by a channel electron multiplier (CEM) coated with CsI to increase the quantum efficiency in the region above 1100 Å. The measured spectra were corrected for relative inverse sensitivity of the spectrometer system consisting of the grating and channel electron multiplier. The relative inverse sensitivity calibration data were obtained by measuring the intensities of emissions from electron impact excitation of molecular hydrogen in the 800–1700 Å range and comparing them to model H_2 intensities [*Ajello et al.*, 1988]. The resulting calibration data and fifth degree polynomial fit are as shown in Figure 1.

[9] At 200 eV electron-impact energy the medium resolution spectrum (1.5 Å FWHM) of electron impact induced fluorescence features of SO_2 was measured from 850 to 1700 Å. The measured spectrum, as shown in Figure 2, consists of emission features from O I, II and S I, II produced by electron impact dissociative excitation and ionization of SO_2. Spectral features in the figure have been identified and numbered as in the work of *Ajello et al.*

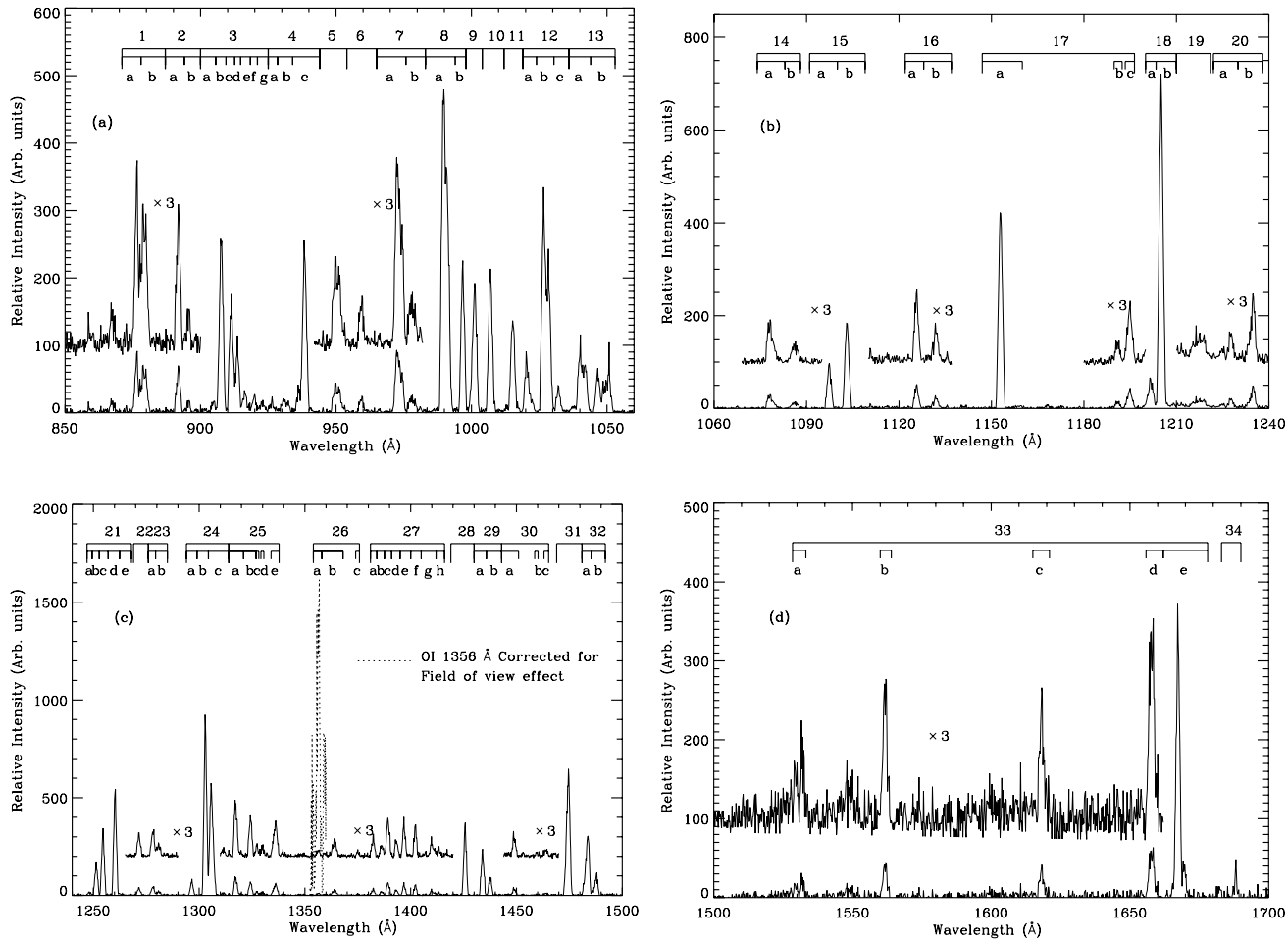

Figure 2. Spectrum of electron impact dissociation of SO_2 by 200 eV electrons. The spectrum was obtained at an instrumental resolution of 1.5 Å in the wavelength range 850–1700 Å. The pressure was 2×10^{-6} torr with an electron beam current of 100 mÅ. Cross sections for the marked spectral features are given in (a) 850–1050 Å, (b) 1050–1250 Å, (c) 1250–1550 Å, and (d) 1550–1750 Å.

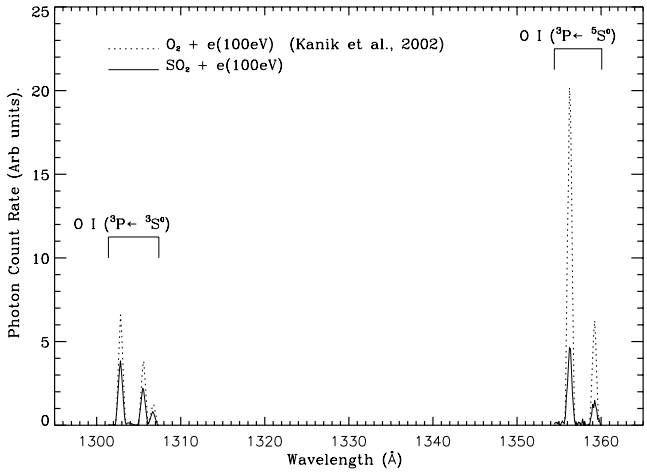

Figure 3. Medium resolution (0.6 Å) spectrum of O I 1304 Å and O I] 1356 Å multiplets from SO_2 with 100 eV electrons. The spectrum from O_2 [*Kanik et al.*, 2003] has been overplotted for comparison. For the optically forbidden O I] 1356 Å multiplet the intensities were corrected for the field-of-view factor. The integrated areas under the peaks were used to estimate the cross sections for O I 1304 Å and O I] 1356 Å.

[1992a] with more subfeatures identified in the present experiment because of the improvement in spectral resolution i.e., 1.5 Å in present experiment vs. 5 Å in the work of *Ajello et al.* [1992a, 1992b]. Cross sections for all the spectral features (excepting Features 14 and 26a) have been estimated by employing as ''bench mark'' the cross section measured at 100 eV electron-impact energy for O I 1304 Å (^3P–^3S) emission from SO_2. The identification for the observed spectral features and their corresponding cross sections are given in Table 1. Since the measured data for relative inverse sensitivity calibration of the spectrometer is applicable only for first order emission spectra, cross sections for the measured second order emission lines could not be estimated. Feature 26a (O I] 1356 Å) required an additional step for estimating the cross section. The need for such an additional step for this particular feature is discussed in section 4.

[10] The procedure for estimating the ''bench mark'' cross section (referred above) is important to describe. This procedure required two separate experiments in which accurate photon count rates were measured for the emission feature O I 1304 Å ($^3P \leftarrow {}^3S$) produced by collision of 100 eV electrons with SO_2 and O_2 molecules respectively. A medium resolution spectrum (600 mÅ FWHM) in the wavelength region 1290–1360 Å (Figure 3) was obtained for SO_2 with electrons of 100 eV energy. Photon count rates for the emissions O I 1304 Å ($^3P \leftarrow {}^3S$) were obtained by integrating the areas under the peaks of their respective fine-structure spectral lines in the measured spectrum. Under similar experimental conditions photon count rates for O I 1304 Å emission was obtained using O_2 as the target gas (Figure 3). The measured photon count rates were corrected for fluctuations in gas density and electron current. The photon count rates were also corrected for the pressure gauge's (A Varian 580 nude ionization gauge was used for measuring pressure in the electron-molecule collision chamber) gas sensitivity factor, which is different for the target gases SO_2 and O_2. As quoted by the manufacturer the gas sensitivity factors (relative to N_2) were 2.2 and 1.05 for SO_2 and O_2, respectively. From the ratio of measured photon count rates and using the recently measured *Kanik et al.* [2003] emission cross section value of $2.9 \pm 0.6 \times 10^{-18}$ cm^2 at 100 eV electron-impact energy for O I 1304 Å from O_2, the ''bench mark'' 100 eV cross section for the O I 1304 Å emission from SO_2 was determined to be $2.3 \pm 0.5 \times 10^{-18}$ cm^2.

[11] A by-product of the above procedure also enabled us to determine the cross section for the optically forbidden O I] 1356 Å ($^3P \leftarrow {}^5S^0$) to be described in section 4. Three major errors contribute to the measured cross sections: (a) the relative uncertainty, 22%, in the O I 1304 Å cross section measured for O_2 by *Kanik et al.* [2003], (b) the error, 4%, due to signal statistics of the strongest features, and (c) the random error, 5%, due to fluctuations in electron gun current and pressure of target gas. For allowed transitions, the root-sum-square of the above three errors gives a relative uncertainty of 23% for the measured cross sections in the present work.

3. Multiplet Structure, Line Profile and Kinetic Energy Distribution Analysis

[12] At 100 and 30 eV electron-impact energies, fine-structure cross sections were studied from the most intense and most important multiplets of S I, II and O I that have been observed by HST with the G140M grating. The cross sections of fine structure lines were measured for each of these multiplets at S II 1256 Å, O I 1304 Å, S I 1429 Å and S I 1479 Å. Line profiles were measured for the strongest atomic oxygen and sulfur fine structure lines at O I 1302.168 Å, O I 1152.151 Å, S I 1473.994 Å and S I 910.485 Å.

3.1. Multiplet Structure at S II 1256 Å, O I 1304 Å, S I 1429 Å, and S I 1479 Å

[13] High-resolution (95 mÅ FWHM) spectra for 100 eV and 30 eV electron energies were measured in the wavelength regions 1290–1320 Å and 1470–1490 Å (see Figures 4a and 4b). Similar measurements were carried out at electron-impact energy of 100 eV for the wavelength regions 1246–1266 Å and 1420–1450 Å (see Figures 4c and 4d). The high-resolution atomic multiplets have been identified and are presented in Table 2.

[14] In Figure 4a the emission at 1304 Å is composed of three fine structure lines. From the standpoint of high resolution measurements in the laboratory the most important multiplet is S I (1479 Å), since it was recently measured by STIS with the G140M grating and analyzed by *Feaga et al.* [2002]. They attributed the observation to excitation of atomic S by ~5 eV electrons. We will show that the intensity distribution of these fine structure lines from SO_2 dissociative excitation is very similar. The multiplet structure is shown in Figure 4b. The multiplet structure is composed of both allowed and forbidden transitions: ($^3P \leftarrow {}^{3,5}D$). We observe in total eight fine structure lines of a possible 13, six allowed and seven optically forbidden transitions. The fine structure lines are numbered 21 through 28. The allowed ones are 22, 23, 25, 26, and 28, while 21, 24, and 27 are intercombination

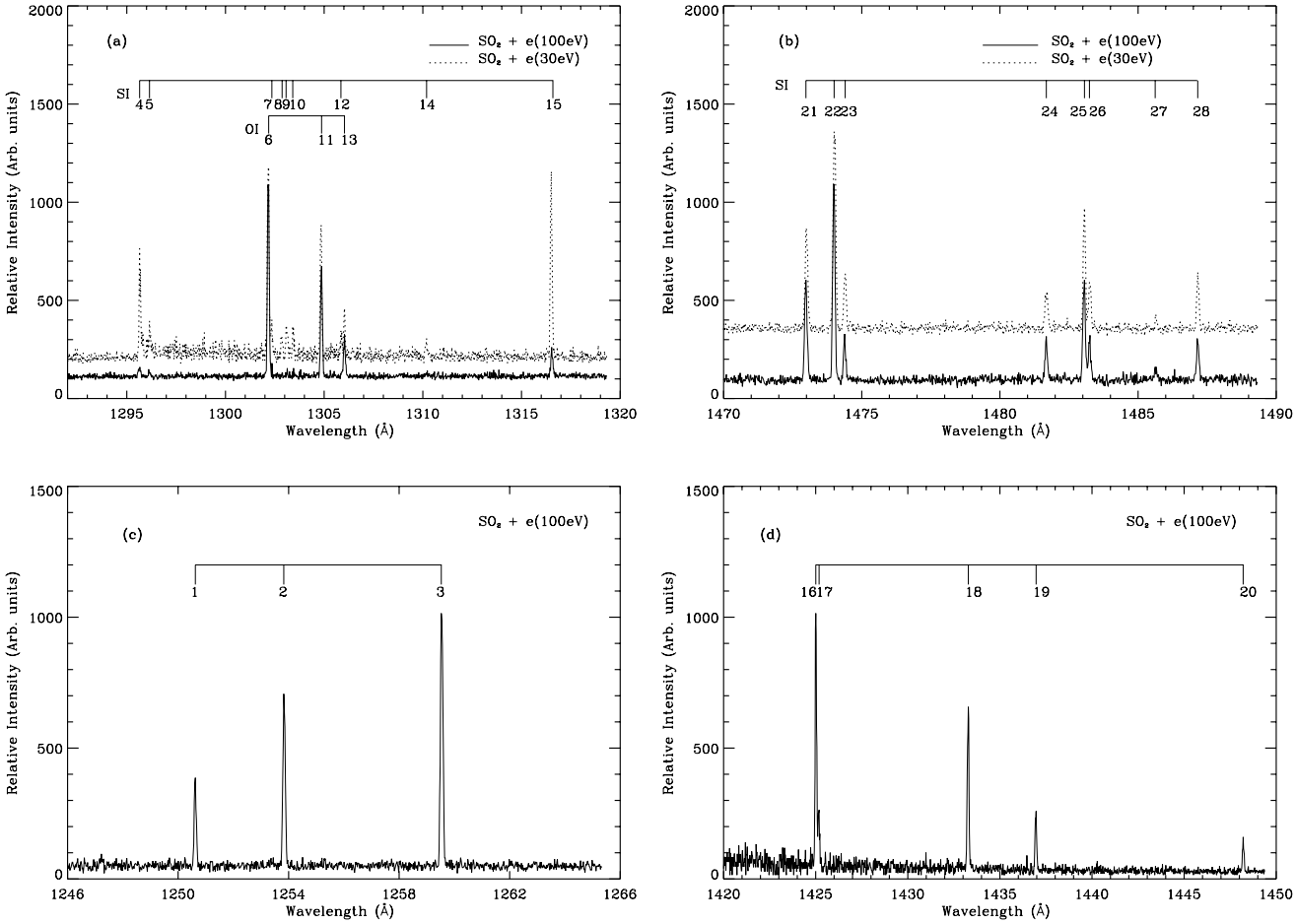

Figure 4. The high-resolution (95 mÅ) spectrum of atomic multiplets from electron impact dissociation of SO_2. Spectra for 100 eV and 30 eV electron energies were measured in the wavelength regions 1290–1320 Å and 1470–1490 Å (a and b). Similar measurements were carried out at electron-impact energy of 100 eV for the wavelength regions 1246–1266 Å and 1420–1450 Å (c and d). The high-resolution atomic multiplets have been identified and are presented Table 2.

lines. The strongest allowed fine-structure feature is numbered 22, which is the transition $^3P_2 \leftarrow {}^5D^0_3$. The strongest optically forbidden fine-structure feature is numbered 21. It is a blend of inter-combination transitions $^3P_2 \leftarrow {}^5D_{3,2,1}$. The cross sections for fine structure lines of the high resolution atomic multiplets were estimated by using the "bench mark" 100 eV cross section of OI 1304 Å from SO_2. We report the cross sections for each of these features in Table 2.

[15] The multiplet at 1256 Å (Figure 4c) is composed entirely of S II fine structure lines from the transition $^4S \leftarrow {}^4P$ Additionally, the contribution of S I multiplets $^3P \leftarrow {}^3S^0$, $^3D^0$ in the wavelength range 1246–1266 Å is found to be negligible [*Ajello et al.*, 1992a]. A multiplet with similar structure but composed of optically allowed fine structure lines is S I 1429 Å. We show this multiplet in Figure 4d. The strongest line is feature 16, which is the transition $^3P_2 \leftarrow {}^3D^0_3$.

3.2. Line Profiles and Kinetic Energy Analysis

[16] Doppler broadened line profiles were measured for certain strongly emitting fine structure lines of atomic sulfur and oxygen produced by crossing the molecular beam of SO_2 with a beam of electrons of energy 100 eV and 30 eV. Evidently, the extent of Doppler broadening depends on the kinetic energies of the atomic fragments dissociated from SO_2 by electron impact. The observed line profile $I(\lambda)$ is a convolution of the true line profile $T(\lambda')$ and the instrumental slit function $A(\lambda - \lambda')$ as shown in the equation below.

$$I(\lambda) = \int T(\lambda')A(\lambda - \lambda')d\lambda'$$

The line profile measurements were carried out with an instrumental slit width of 20 μm. Instrumental slit functions were measured for the present experimental set-up. The measured FWHM for instrumental slit were 36 mÅ and 24 mÅ respectively for second order and third order. Line profile measurements were carried out for O I 1302.168 Å ($^3P_2 \leftarrow {}^3S^0_1$), O I 1152.151 Å ($^1D_2 \leftarrow {}^1D^0_2$), S I 1473.994 Å ($^3P_2 \leftarrow {}^3D^0_3$), and S II 910.485 Å ($^4S^0_{3/2} \leftarrow {}^4D_{3/2}$). The optically forbidden O I] 1355.598 Å ($^3P_2 \leftarrow {}^5S^0_2$) line could not be measured due to poor signal-to-noise ratio. The line profile measurements were carried out either in second order or third order. The choice of the spectral order depended primarily on the limitations set by grating rotation

Table 2. Transition Terms and Cross Sections for Atomic Multiplets Identified From Figure 3[a]

Feature	Integrated Wavelength Interval (Å)	Wavelength (Å)	Transition Terms	Cross Section (10^{-18} cm^2) 100 eV	30 eV
1	1250.52–1250.88	1250.816	S I $^3P_0 \leftarrow {}^3S_1$	0.200	
		1250.584	S II $^4S^0_{3/2} \leftarrow {}^4P_{1/2}$		
2	1253.66–1253.98	1253.811	S II $^4S^0_{3/2} \leftarrow {}^4P_{3/2}$	0.540	
3	1259.40–1259.68	1259.519	S II $^4S^0_{3/2} \leftarrow {}^4P_{5/2}$	0.550	
4	1295.53–1295.75	1295.653	S I $^3P_2 \leftarrow {}^3P^0_2$	0.120	0.054
5	1295.75–1296.33	1296.174	S I $^3P_2 \leftarrow {}^3P^0_2$	0.170	0.054
6	1302.03–1302.31	1302.168	O I $^3P_2 \leftarrow {}^3S^0_1$	1.280	0.120
7	1302.33–1302.47	1302.336	S I $^3P_1 \leftarrow {}^3P^0_2$	0.066	0.017
8	1302.75–1302.95	1302.862	S I $^3P_1 \leftarrow {}^3P^0_1$	0.055	0.018
9	1303.01–1303.23	1303.110	S I $^3P_2 \leftarrow {}^3P^0_1$	0.074	0.025
10	1303.35–1303.53	1303.430	S I $^3P_2 \leftarrow {}^3S^0_1$	0.067	0.020
11	1304.75–1305.01	1304.858	O I $^3P_1 \leftarrow {}^3S^0_1$	0.730	0.074
12	1305.79–1305.91	1305.884	S I $^3P_0 \leftarrow {}^3P^0_1$	0.049	0.014
13	1305.91–1306.13	1306.029	O I $^3P_0 \leftarrow {}^3S^0_1$	0.290	0.030
14	1310.07–1310.35	1310.194	S I $^3P_1 \leftarrow {}^3S^0_1$	0.100	0.020
15	1316.30–1316.69	1316.622	S I $^3P_2 \leftarrow {}^3D^0_1$	0.280	0.12
		1316.615	S I $^3P_2 \leftarrow {}^3D^0_2$		
		1316.542	S I $^3P_2 \leftarrow {}^3D^0_3$		
16	1424.86–1425.10	1425.030	S I $^3P_2 \leftarrow {}^3D^0_3$	0.049	
17	1425.10–1425.32	1425.219	S I $^3P_2 \leftarrow {}^3D^0_1$	0.015	
		1425.188	S I $^3P_2 \leftarrow {}^3D^0_2$		
18	1433.12–1433.44	1433.310	S I $^3P_1 \leftarrow {}^3D^0_1$	0.036	
		1433.278	S I $^3P_1 \leftarrow {}^3D^0_2$		
19	1436.84–1437.06	1436.963	S I $^3P_0 \leftarrow {}^3D^0_1$	0.013	
20	1448.10–1448.30	1448.230	S I $^1P_2 \leftarrow {}^1D^0_2$	0.007	
21	1472.86–1473.12	1473.070	S I] $^3P_2 \leftarrow {}^5D^0_1$	0.520	0.320
		1473.019	S I] $^3P_2 \leftarrow {}^5D^0_2$		
		1472.971	S I] $^3P_2 \leftarrow {}^5D^0_3$		
22	1473.84–1474.14	1473.994	S I $^3P_2 \leftarrow {}^3D^0_3$	0.950	0.640
23	1474.28–1474.52	1474.378	S I $^3P_2 \leftarrow {}^3D^0_2$	0.200	0.160
		1474.571	S I $^3P_2 \leftarrow {}^3D^0_1$		
24	1481.56–1481.78	1481.713	S I] $^3P_1 \leftarrow {}^5D^0_1$	0.200	0.120
		1481.663	S I] $^3P_1 \leftarrow {}^5D^0_2$		
25	1482.94–1483.16	1483.038	S I $^3P_0 \leftarrow {}^5D^0_1$	0.510	0.320
26	1483.16–1483.38	1483.233	S I $^3P_0 \leftarrow {}^3D^0_1$	0.210	0.140
27	1485.48–1485.78	1485.622	S I] $^3P_0 \leftarrow {}^5D^0_1$	0.075	0.018
28	1487.06–1487.30	1487.150	S I $^3P_0 \leftarrow {}^3D^0_1$	0.210	0.140

[a]The values given here up to four significant figures serve to indicate the relative magnitudes of the various features. They do not represent the accuracy of the individual one.

(the 3-m spectrometer the maximum grating rotation angle is 8° which corresponds to a maximum wavelength of 3700 Å) and the signal-to-noise ratio of the measured intensities of the emitted line radiation.

[17] The true emission profiles could be obtained by deconvoluting the observed line profile with the appropriate slit function. The mathematical FFT technique of deconvolution used for the present analysis has been fully described in earlier publications [*Ajello et al.*, 1995a, 1995b]. Low pass step filter [*Press et al.*, 1986] was used to eliminate high frequency noise in the data and thus prevent spectral leakage into the side lobes of deconvoluted profiles. Filtered observed line profiles, slit functions and the de-convoluted line profiles are shown in Figure 5. The line profiles (measured and true) and slit functions are all approximately gaussian in form. The resultant FWHM values of line profile analysis are presented in Table 3. The square root of the sum of squares of the FWHM of the true line profile and slit function is approximately equal to the FWHM of the measured profile. As may be seen from Figures 5c and 5d and Table 3, in the case of S II 910.485 Å, S I 1473.994 Å and O I 1302.168 Å at 30 eV the measured line widths are comparable to the slit function. Therefore deconvolution procedure was not successful for these measured line profiles and only upper limits to the average kinetic energy distributions could be established.

[18] Deconvoluted data was used to calculate the kinetic energy distribution of oxygen atoms. The kinetic energy distribution $P(E)$ is given by

$$P(E) = k\frac{dT}{d\lambda},$$

where k is a multiplicative constant [*Ogawa and Higo*, 1979, 1980; *Ogawa et al.*, 1992]. In the cases of O I 1302.168 Å and O I 1152.151 Å the resultant kinetic energy distribution for 100 eV electrons are shown in Figure 6. Peak values and mean values for the kinetic energy were determined for the above distributions and are presented Table 4. The data for excited O I atoms from O_2 experiments by *Makaraov et al.* [2002] have also been included for comparison. The largest peak kinetic energy observed was 2.0 eV at 1152.151 Å for an O (^{1}D) atom.

[19] Since deconvoluted line profiles were not available for S II 910.485 Å, S I 1473.99 Å and O I 1302.168 Å at 30 eV their corresponding kinetic energy distributions could not be produced. However, we attempt here to estimate an upper limit for their average kinetic energies, *KE*, from the

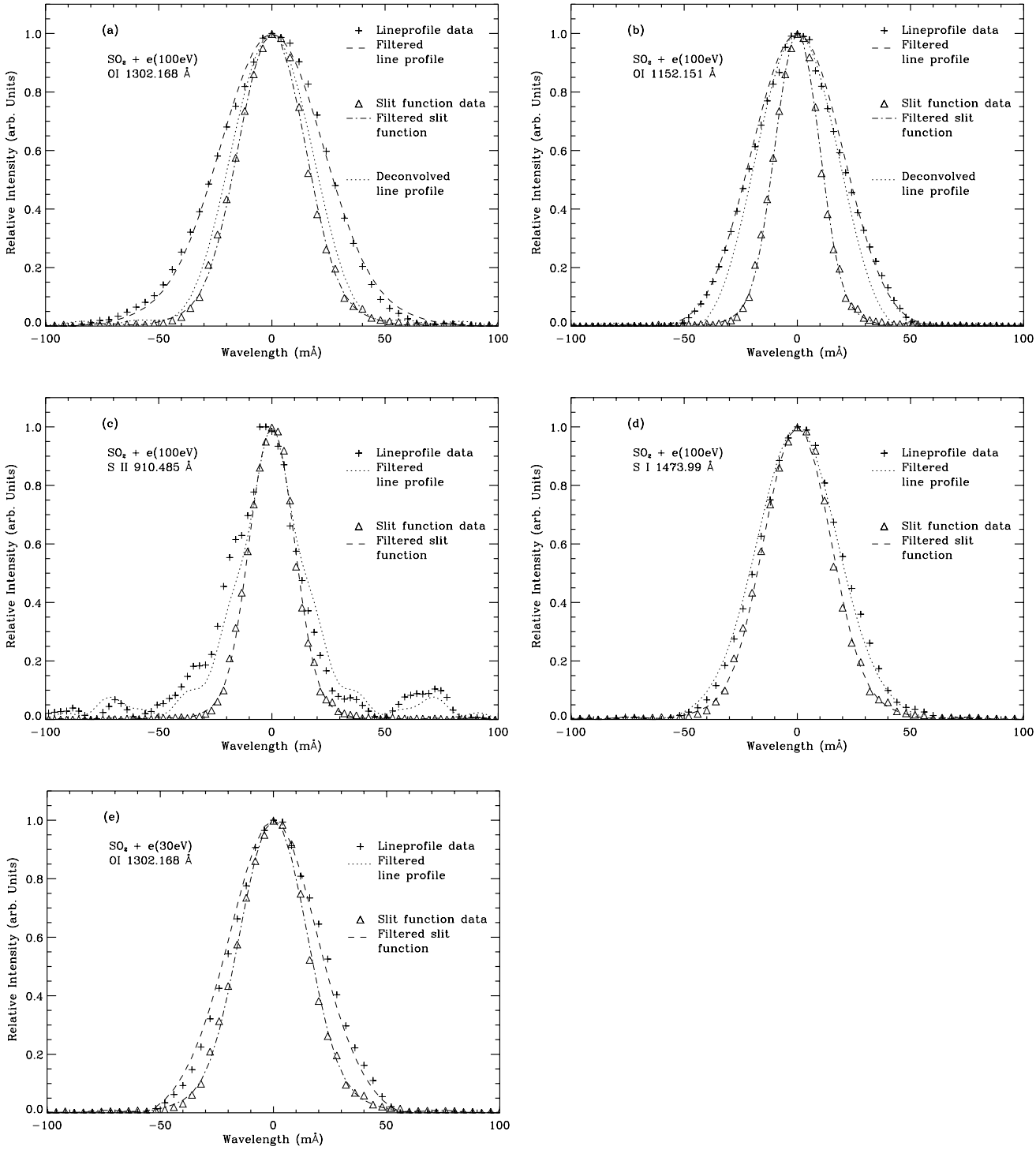

Figure 5. The Doppler line profiles for atomic oxygen and sulfur produced by electron impact with SO_2. The line profiles were obtained using slit width of 20 μm. Deconvoluted line profiles were obtained for (a) O I 1302.168 Å and (b) O I 1152.151 Å with 100 eV electrons. De-convolution was not possible for (c) S II 910.485 Å and (d) S I 1473.99 Å with 100 eV electrons and for (e) O I 1302.168 Å with 30 eV. The FWHM data for the measured line profiles, slit functions and de-convoluted line profiles are presented in Table 3.

Table 3. Measured and Deconvoluted Doppler Line Widths for Fine Structure Lines of Atomic Oxygen and Sulfur Produced By Electron Impact With SO_2[a]

Spectral Line	Energy (eV)	Spectral Order	Slit Function FWHM (mÅ)	Spectral Line Width (mÅ)		
				Measured	Deconvolved	Estimated[b]
S II 910.4850 Å	100	third	24.0 ± 4.0	33.0 ± 8.0		22.5 ± 9.0
O I 1152.151 Å	100	third	24.0 ± 4.0	46.0 ± 8.0	39.5 ± 7.0	39.0 ± 9.0
O I 1302.168 Å	100	second	36.0 ± 6.0	55.0 ± 8.0	40.5 ± 5.0	41.0 ± 10.0
O I 1302.168 Å	30	second	36.0 ± 6.0	46.0 ± 8.0		29.0 ± 10.0
S I 1473.990 Å	100	second	36.0 ± 6.0	43.0 ± 8.0		35.0 ± 10.0

[a]The FWHM data for the slit functions (used for deconvolution) are included. The line profiles and slit functions are shown in Figure 5.
[b]Estimated from the square root of difference of squares of measured and slit function line widths.

FWHM values of the filtered observed line profiles. The nonrelativistic Doppler shift, $\Delta\lambda$ in Å, is given by

$$\Delta\lambda = 4.62 \times 10^{-5}\sqrt{\frac{KE}{M}}\lambda_0 \, \mathrm{Cos}\,\theta_0,$$

where KE is the kinetic energy of the atomic fragment in eV, M is the mass of the atomic fragment in A.M.U. and λ_0 is the emitted central wavelength in Å. Considering an observation along the line of sight of the spectrometer, $\theta = 0°$, and with $\Delta\lambda$ = (FWHM ÷ 2) of the filtered observed line profile, the upper limit for the kinetic energy was estimated. Similarly, upper limits were also estimated for O I 1302.168 Å and O I 1152.151 Å at 100 eV, whose values, as seen in Table 4, agree well with their corresponding mean kinetic energies within the limits of the experimental uncertainty. We consider here the model reaction where the SO_2 molecule, upon electron impact, dissociates to produce a single sulfur atom and two oxygen atoms. A simplified approach based on the principles of conservation of momentum and energy was adopted to understand the dissociation process. Regardless of the O - S - O bond-angle present at the instant of dissociation it was found that the velocities of sulfur atoms were always either lesser than or equal to the velocities of oxygen atoms.

4. The O I] 1356 Å ($^3P \leftarrow {}^5S^0$) Cross Section

[20] A straightforward extension of the procedure in section 2 for measuring the absolute cross section of O I] 1356 Å would not be possible owing to its long radiative lifetime (180 μs). Due to the long radiative lifetime, a substantial fraction of the excited O ($^5S^0$) atoms escape detection by drifting away from the finite field of view of the 3-m spectrometer before emitting the radiation. For the O I] 1356 Å radiation, an estimated mean kinetic energy of 2 eV for the excited O ($^5S^0$) atoms produced at 100 eV electron impact energy is sufficient to cause them to drift out of the field of view, 1.49°, of the 3-m spectrometer. A correction factor (here after referred to as the field-of-view factor) was required to account for the above effect before an accurate value of the 100 eV cross section could be determined. The field-of-view factor (for O_2 experiments) relevant to the present experimental set-up was obtained by comparing the ratio of O I] 1356 Å/O I 1304 Å cross sections at 100 eV in the same way as obtained in an earlier measurement by *Kanik et al.* [2003] with the ratio of measured (present) integrated intensities of the corresponding spectral lines of Figure 3. In the O_2 experiment a value of 103 was obtained for the field-of-view factor. Which means only 1/103 of the O I] 1356 Å emission was observed in our apparatus compared to an allowed transition. We will show that the field-of-view factor determined for the present experimental set-up for O I] 1356 Å from O_2 can also be used for O I] 1356 Å from SO_2. The field-of-view factor is accurate provided that the excited O I atoms have the same mean kinetic energies for the two different parent molecules.

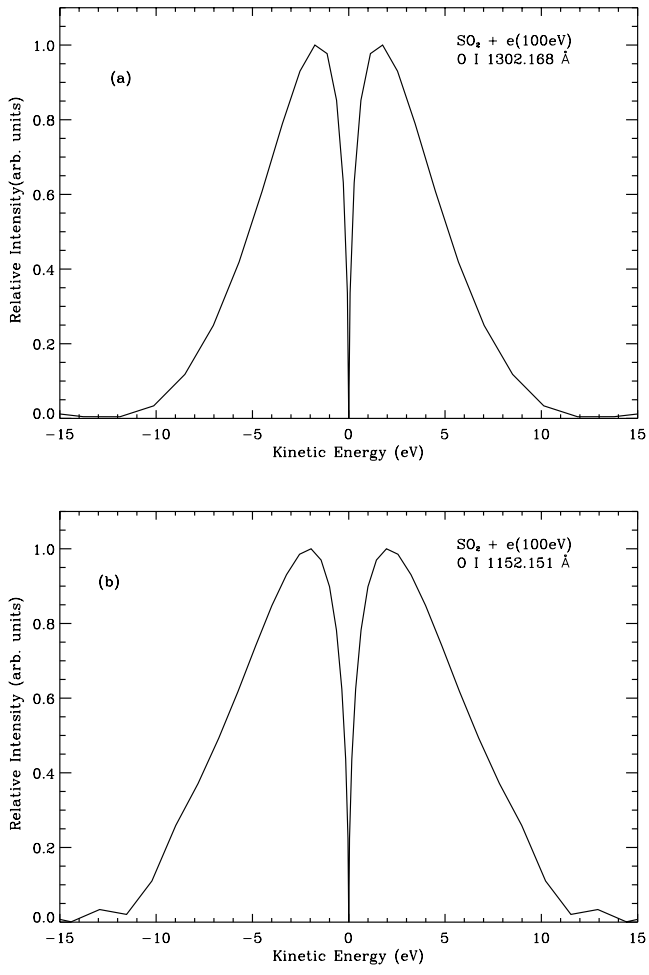

Figure 6. Kinetic energy distributions (a) of O I 1302.168 Å and (b) of O I 1152.151 Å, for excited O I atoms were derived from their respective (de-convolved) line profiles of Figures 5a and 5b. The peak KE, mean KE and the estimated upper limits for KE of these distributions are presented in Table 4.

Table 4. Peak K.E., Mean K.E., and Estimated Upper Limits for Average Kinetic Energies of Excited O I and S I Atoms Produced From SO_2 (Present Study)[a]

	SO_2 + e (100 eV)			O_2 + e (100 eV)		SO_2 + e (30 eV)
Spectral Line	Peak KE (eV)	Mean KE (eV)	Upper Limit for KE (eV)	Peak KE (eV)	Mean KE (eV)	Upper Limit for KE (eV)
S II 910.485 Å			2.3 ± 1.8			
O I 1152.151 Å	2.0 ± 0.8	3.0 ± 1.3	2.2 ± 1.2	2.1 ± 0.3	4.0 ± 0.6	
O I 1302.168 Å	1.8 ± 0.5	2.4 ± 1.2	1.8 ± 0.9	0.6 ± 0.3	2.5 ± 1.2	0.92 ± 0.6
O I] 1355.598 Å				1.3 ± 0.5	2.4 ± 1.0	
S I 1473.990 Å			2.2 ± 1.2			

[a]The peak and mean kinetic energy for O I atoms from O_2 *Makarov et al.* [2003] are compared.

The mean kinetic energy for O ($^3S^0$) is estimated from the line profile intensities for O I 1302.168 Å. The kinetic energy distribution results for SO_2 are listed in Table 4. The mean kinetic energy value of 2.4 eV was compared with that of O_2 [*Makarov et al.*, 2003; *Kanik et al.*, 2003]. We have found that the kinetic energies estimated from O I 1302.168 Å line profiles for SO_2 and O_2 are nearly same (i.e., within the measurement uncertainties). Also, the O_2 data indicate that the estimated kinetic energies are the same (within experimental uncertainties) for O I 1302.168 Å and O I] 1355.598 Å line profiles. Therefore within the limits of measurement uncertainties, we assume that the excited O ($^{3,5}S^o$) atoms produced from SO_2 and O_2 have equal kinetic energies. This is the basic assumption in this work until we can measure the fine structure profile. We were not able to directly estimate the mean kinetic energy of O ($^5S^o$) since its high-resolution line profile measurement yielded low count rates. We expect to use much longer integration time in the future.

[21] The measured photon intensity for O I] 1356 Å from SO_2 was corrected by applying the field-of-view factor and is shown in the Figure 3. From the estimated cross section value of $2.3 \pm 0.5 \times 10^{-18}$ cm^2 for O I 1304 Å from SO_2 and the measured ratio of photon count rates for O I 1304 Å/O I] 1356 Å (see Figure 3), the cross section for O I] 1356 Å from SO_2 was found to be $2.1 \pm 1.0 \times 10^{-18}$ cm^2. It may be noted here that feature 26a identified in Table 1, belongs to the optically forbidden transitions of the spectral feature O I] 1356 Å produced by the collision of 200 eV electrons with SO_2. Since it was not possible to estimate the field-of-view factor for 200 eV measurements, we corrected the measured intensities of feature 26a in Figure 2 by using the O I] 1356 Å cross section at 200 eV from the excitation function data given in section 5. Thereby, a correct estimate of the cross section for feature 26a was obtained. Apart from the errors quoted for cross sections in section 2 (for the allowed transitions), in the case of the forbidden transition O I] 1356 Å, the field-of-view factor contributes an estimated additional error of ~40%. Therefore for O I] 1356 Å cross section, the relative uncertainty (root-sum-square of errors) becomes ~46%.

5. Optical Excitation Function Measurements

[22] Electron impact induced emission cross sections for optically allowed transition at O I 1304 Å and optically forbidden transition at O I] 1356 Å were obtained on the JPL 3 m high-resolution spectrometer over the electron impact energy range 0–800 eV. The excitation function (relative cross section) data for the transition at O I 1304 is shown in Figure 7a. Three dominant dissociation and ionization processes could be identified from the data, they are, Process I: $SO_2 + e \rightarrow O^* + SO$, Process II: $SO_2 + e \rightarrow O^* + SO^+$, and Process III: $SO_2 + e \rightarrow O^* + O^+ + S$. The values of measured appearance potentials (measured thresholds) W and their corresponding theoretical thresholds W_{th} are given in Table 5.

[23] The measured relative excitation cross sections for the transition O I 1304 Å were put on absolute scale by normalizing them to the cross section value of 2.28×10^{-18} cm^2 at 100 eV. The measured O I 1304 Å cross sections are fitted through the semiempirical relation [*Jackman et al.*, 1977; *Bhardwaj and Michael*, 1999b]

$$\sigma(E) = \frac{q_0 F}{W^2}\left[1 - \left(\frac{W}{E}\right)^{\alpha}\right]^{\beta}\left(\frac{W}{E}\right)^{\Omega},$$

where $q_0 = 4\pi a_0^2 R^2$ and has the numerical value 6.513×10^{-14} eV^2 cm^2. The cross section $\sigma(E)$ is a sum of the contributions from the three independent processes I, II, and III. The fit parameters for these processes are given in Table 5. The model-fit curve is shown in Figure 7a.

[24] Polarization effects are unimportant for the measurement of excitation functions from SO_2 atomic products from dissociation. Many excited repulsive intermediate states contribute to the emission multiplets from excited atoms observed in this paper. The large number of intermediate states will diminish the anisotropic distribution of fragments and the associated polarization [*van Brunt and Zare*, 1968]. In addition, the polarization of radiation from the excited $^{3,5}S$ states for 130.4 and 135.6 nm, respectively, is zero.

[25] As described in section 4, it is required to correct the O I] 1356 Å excitation data for the field-of-view factor. The field-of-view factor is inversely proportional to the mean velocity (or in other words the inverse square root of mean kinetic energy) of the distribution function for atomic species emitting the optically forbidden spectral line [*Ajello*, 1970]. Each process involved in the dissociation and ionization (i.e., processes I, II, and III) produces its own characteristic velocity distribution. The fractional contribution of each of these causes the field-of-view factor to be dependent on the electron impact energy. The estimated value for 100 eV (in section 4) cannot be used to correct the entire range of data from threshold to 800 eV. It is therefore essential to know the variation of the field-of-view factor

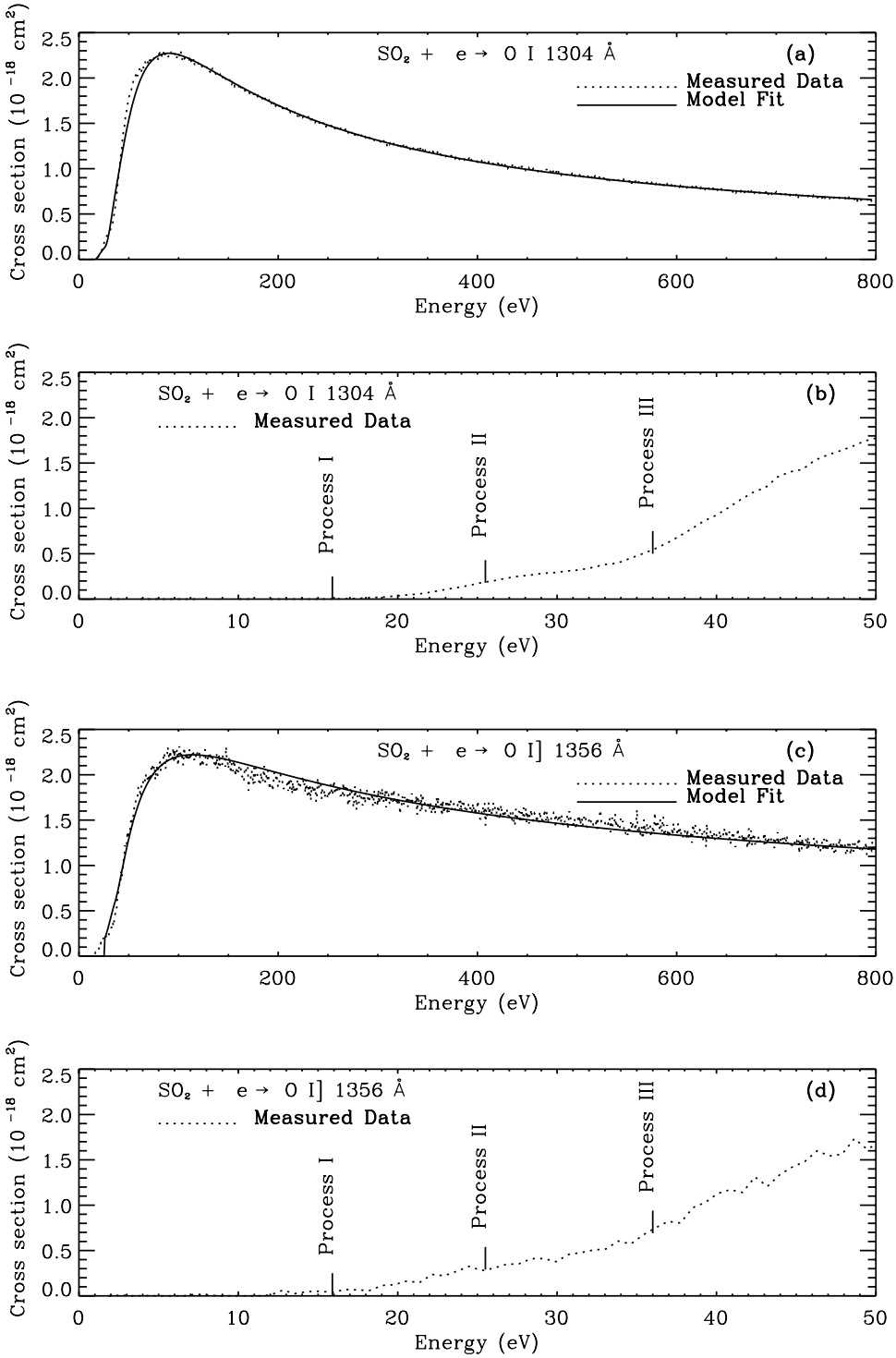

Figure 7. The measured excitation function for (a and b) O I 1304 Å and (c and d) O I] 1356 Å. The data were measured at a spectral resolution of 6.5 Å with the experimental settings satisfying optically thin conditions. The fit parameters for the modified Born approximation model are given in Table 5. Identifications for the processes I, II and III (indicated at their measured thresholds) in the near threshold excitation for (Figure 7b) O I 1304 Å and (Figure 7d) O I] 1356 Å are given in section 5.

with respect to the electron-impact energy. We built a smooth function representing the variation of field-of-view factor w.r.t the electron-impact energy by using (a) the measured mean values of kinetic energies of the O ($^3S^0$) atoms produced by 100 eV and 30 eV electrons (see Table 4) and (b) fractional contribution of the three dissociation processes (I, II, and III) at each electron impact energy to the measured O I 1304 Å cross section. The summation of these fractional contributions was possible since each dissociation process produces a unique kinetic energy distri-

Table 5. Model Fit Parameters for $SO_2 + e \rightarrow$ O I 1304 Å and O I] 1356 Å

Parameter	O I 1304 Å			O I] 1356 Å		
Process	I	II	III	I	II	III
W	15.9 eV	25.5 eV	36.0 eV	15.5 eV	25.5 eV	36.0 eV
α	0.25	1.5	1.5	0.25	1.5	1.5
β	2.1	2.9	2.9	2.1	2.1	2.1
Ω	1.7	1.75	0.7	1.7	0.7	0.38
F	0.11	0.125	0.11	0.15	0.025	0.062
W_{th}	15.2 eV	25.24 eV	34.26 eV	14.83 eV	24.87 eV	33.89 eV

bution. For example, below 25 eV only dissociation into neutral species occurs with a mean kinetic energy of less than 0.9 eV (Table 4) while above 100 eV dissociative ionization dominates the contribution to the 2.4 eV kinetic energy. The measured excitation data for O I] 1356 Å were then corrected by using this function.

[26] The measured relative excitation cross sections for the transition O I] 1356 Å were put on absolute scale by normalizing them to the cross section value $2.1 \pm 1 \times 10^{-18}$ cm^2 at 100 eV. A model fit for the corrected O I] 1356 Å cross sections was obtained using the same procedure as described in the case of O I 1304 Å. The fit parameters are given in Table 5. The model-fit curve for O I] 1356 Å is shown in Figure 7c.

[27] Cross sections for O I 1304 Å and O I] 1356 Å as a function of energy in the range 0–800 eV are given in Table 6. From the optical excitation data we obtain the ratio of O I 1304 Å/O I] 1356 Å cross section as a function of energy in the range 0–800 eV and this ratio is shown in Figure 8.

6. Discussion

[28] We have measured the optically thin combined EUV and FUV spectrum of e (200 eV) + SO_2 at medium (1.5 Å FWHM) and of e (30,100 eV) + SO_2 high resolution (less than 0.1 Å FWHM). The medium resolution results can be compared to the low resolution *Ajello et al.* [1992a] for the same electron impact energy of 200 eV. In general the cross sections agree within 25% as shown in Table 1. In total we have identified about 120 features over the wavelength range 800–1700 Å compared with the 61 features previously identified [*Ajello et al.*, 1992a] encompassing the wavelength range from 400–2000 Å. We have resolved sub-intervals on a finer basis (1.5 Å FWHM versus 5 Å FWHM). Based on our current results we have established that the O I 1304 Å and O I] 1356 Å multiplets are the two strongest features in the UV spectrum of SO_2, followed closely in intensity or cross section by S I 1479 Å. The strongest S I feature arises from a combination of allowed and forbidden transitions. We have established the cross section of the O I 1304 Å multiplet at 100 eV as $2.3 \pm 0.50 \times 10^{-18}$ cm^2. High-resolution studies of the O I 1304 Å multiplet show the contributions from blended S I features are negligible. At 100 eV electron-impact energy, we give a preliminary estimate of the cross section for the optically forbidden O I] 1356 Å emission from SO_2 as $2.1 \pm 1.0 \times 10^{-18}$ cm^2.

[29] Observations of Io have been obtained periodically via HST since 1992. The first observations used the Faint Object Spectrograph (0.6 Å–12 Å FWHM) to obtain a complete FUV spectrum of the Io airglow viewed through the torus foreground of Iogenic emissions [*Clarke et al.*, 1992]. In 1995–1996 GHRS captured the rich spectra of S and O lines, illustrated in Figures 9a and 9b), operating at 3.5 Å FWHM with the G140L grating (M. A. McGrath, private communication, 2003). The strong multiplets from O I 1304 Å, O I] 1356 Å and S I 1479 Å stand out as the most intense just as in the laboratory spectrum of SO_2. The ratio of the line intensities of 1304 Å to 1356 Å in Figure 9 (top) and Figure 9 (bottom) show a variable ratio of 2.0 to 0.8, respectively, for these observations. This ratio can be expected to be variable for a number of reasons. First, we show in Figure 8 and Table 6 that the cross section ratio can vary substantially with mean electron impact energy in the low region (17.5–40 eV). This ratio is 0.3 and 1.3, respectively, for 17.5 and 40 eV. In addition, the column densities of oxygen-bearing species in the Io atmosphere have a large diurnal and latitudinal variation and their densities also depend on the relative contribution of subli-

Table 6. Emission Cross Sections for S I 1479 Å, O I 1304 Å, and O I] 1356 Å From SO_2[a]

Electron	Cross Section (10^{-18} cm^2)			Field-of-View
Energy (eV)	S I 1479 Å	O I 1304 Å	O I] 1356 Å	Factor
17.5	0.0	0.012	0.041	61.8
20	0.097	0.040	0.092	61.8
22.5	0.257	0.091	0.144	61.8
25	0.510	0.192	0.188	61.8
27.5	0.732	0.242	0.218	61.8
30	0.933	0.304	0.259	61.8
32.5	0.999	0.367	0.318	61.8
35	1.018	0.475	0.386	61.8
37.5	1.028	0.737	0.513	63.9
40	1.052	0.974	0.770	67.0
42.5	1.068	1.145	0.871	71.1
45	1.153	1.490	1.088	75.2
47.5	1.197	1.624	1.209	79.3
50	1.205	1.780	1.320	82.4
52.5	1.380	1.895	1.490	85.5
55	1.445	1.986	1.624	87.6
57.5	1.477	2.065	1.751	89.6
60	1.520	2.080	1.858	90.6
65	1.574	2.140	1.935	93.7
70	1.585	2.198	1.950	95.8
75	1.607	2.236	2.044	97.8
80	1.617	2.250	2.131	99
85	1.628	2.300	2.235	99.9
90	1.639	2.267	2.194	100.9
95	1.628	2.277	2.240	102.0
100	1.618	2.280	2.140	103.0
150	1.553	1.990	2.105	103.0
175	1.467	1.895	1.937	103.0
200	1.348	1.713	1.872	103.0
225	1.262	1.587	1.928	103.0
250	1.122	1.481	1.774	103.0
275	1.078	1.395	1.698	103.0
300	0.985	1.325	1.745	103.0
350	0.907	1.193	1.670	103.0
400	0.789	1.089	1.670	103.0
450	0.725	0.997	1.536	103.0
500	0.627	0.940	1.457	103.0
550	0.604	0.868	1.360	103.0
600	0.554	0.832	1.370	103.0
650	0.519	0.764	1.331	103.0
700	0.479	0.737	1.249	103.0
750	0.435	0.693	1.218	103.0
800	0.423	0.644	1.191	103.0

[a]The values given here up to four significant figures serve to indicate the relative magnitudes of the various features. They do not represent the accuracy of the individual one.

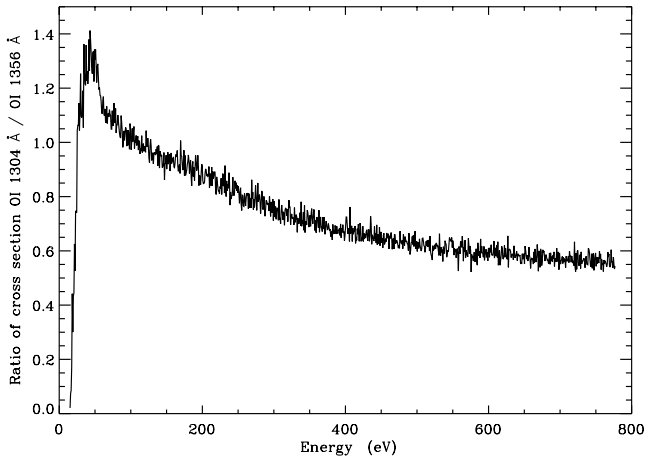

Figure 8. The ratio of O I 1304 Å/O I] 1356 Å emission cross sections as a function of energy.

mation to volcanic activity in driving the atmosphere [*Wong and Smyth*, 2000; *Moses et al.*, 2002]. Each of these species has a unique cross section ratio dependence for 1304 Å/1356 Å in the low energy region (Kanik et al., submitted manuscript, 2004). A weighted average of these two effects could contribute to the observed variation.

[30] More recently, making use of the resolving power of the G140M grating with STIS, it was possible to study the multiplet fine structure of S I 1479 Å at 0.5 Å FWHM [*Feaga et al.*, 2002]. The low and medium resolution spectra acquired by spacecraft have shown the need for high-resolution laboratory spectra for comparison beyond that achieved by *Ajello et al.* [1992a, 1992b] (5 Å FWHM). This paper represents the first step in that direction. The Io FUV airglow spectrum is primarily produced by electron impact of S, O, and SO_2. An electron temperature of 5 eV with a nonthermal and variable high-energy tail component characterizes the undisturbed torus plasma distribution function of electrons. The 5 eV thermal distribution is capable of directly exciting UV resonance lines from S and O atoms. On the other hand, if a component of the observed emission from any of the multiplets originate from dissociative excitation of a molecule, then the multiplets require electrons of at least 15 eV electron impact energy to produce the same emission lines from dissociative excitation of SO_2 or SO. However, the first threshold near 15 eV is not considered strong enough to produce the observed intense emissions at Io. The intense emissions would occur at energies above 25 eV as the second and third thresholds listed in Table 5 become available for the "hot" distribution tail. The Plasma (PLS) instrument on Galileo has the capability to measure fluxes of field-aligned electrons with a distribution of energies from 0.9 eV to 52 keV [*Frank and Paterson*, 1999, 2002; cf. *Oliversen et al.*, 2001]. Recently, *Oliversen et al.* [2001] have noted a sporadic integrated intensity and non-thermal line broadening emission from O I (6300 Å). Dissociative excitation of SO_2 by high-energy electrons could explain these phenomena. It is probable that both dissociative excitation of SO_2 and direct excitation of atomic S and O contribute to the neutral emission lines.

[31] A final application of our results can be applied to the 1997 STIS observations of *Roesler et al.* [1999]. We compare in Table 7 the observed in intensities of the atomic S and O FUV multiplets with the cross section ratios for these same features at 3 Rydbergs (~40 eV) for SO_2 and 1 Rydberg (14 eV) for atomic S. The cross sections were normalized to S I 1479 Å cross section by taking its value as 1.99. The STIS observations (except for S I 1389 Å) can be fully matched by our e + SO_2 cross sections at 3 Rydbergs. However, the e + S total (allowed + forbidden) cross sections near 1 Rydberg for the 1479/1429 ratio studied by *Zatsarinny and Tayal* [2001, 2002] also matches the data. The intensity of the STIS SI 1389 Å multiplet is better matched with a process of e + S. It is not possible to identify the dominant emitting species solely on the basis of UV spectroscopy alone. A model of the energy dependent electron flux and atmospheric column densities at Io can be best utilized to answer this question.

[32] To better understand the high-resolution multiplet structure produced from both e + S and e + SO_2 at 100 eV in the Born region we compare the multiplet structure of S I (1479 Å) from both processes. The e + S optically thin model spectrum for this multiplet was shown previously [*Feaga et al.*, 2002]. The e + SO_2 optically thin spectrum was shown earlier in Figure 6b at 0.095 Å FWHM. We can compare the fine structure distribution in Figure 10a at 0.235 Å FWHM, where the allowed and forbidden components of the e + S spectrum are separately normalized at 1474 Å at 1473 Å, respectively. The two spectra are indistinguishable. We show the same effect at higher resolution of 0.09 Å FWHM in Figure 10b, where only the

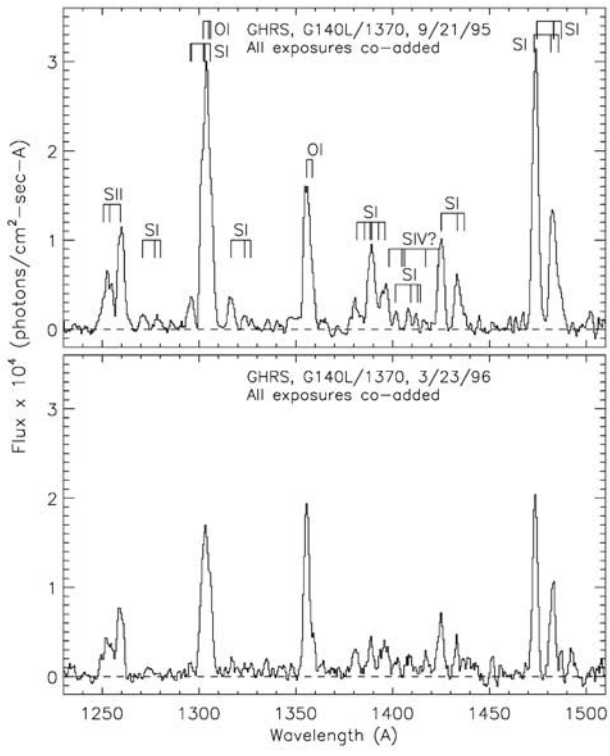

Figure 9. HST GHRS spectra of Io taken with 3.5 Å spectral resolution is shown. The prominent O I 1304 Å and O I] 1356 Å features are easily identified.

Table 7. A Comparison of the Fluxes for O and S Multiplets Measured by HST/STIS for Io [*Roesler et al.*, 1999] With Cross Section Data for SO_2 + e(40 eV) (See Section 4) and the Theoretically Calculated Cross Sections for S + e (1 and 3 Ryd) by *Zatsarinny and Tayal* [2001, 2002][a]

Spectral Lines Observed by STIS	Flux (10^{-3} Photons cm^{-2} Sec^{-1})	SO_2 + e(40 eV)			Ratios of Cross Sections	
		Features Included	Wavelength Range (Å)	Ratios of Cross sections	S + e(1Ryd)	S + e(3Ryd)
O I + S I 1300 Å	1.75	24	1294–1314	1.85		
O I] 1356 Å	1.6	26a	1354–1358	1.45		
S I 1389 Å	1.27	27	1381–1416	0.46	0.88	0.8
S I 1429 Å	1.03	28 and 29	1419–1430	0.88	0.61	2.37
			1430–1443			
S I 1479 Å	1.99	31 and 32	1469–1481	1.99	1.99	1.99
			1481–1492			

[a]In order to enable an easy comparison with the HST/STIS observations the cross sections were normalized to S I 1479 Å cross section by taking its value as 1.99.

allowed transitions are modeled. Each of the J-levels of the upper state ^3D emits spectra of the same relative intensity whether the parent species is S or SO_2. The reason for this similarity in electron-excited emission spectra has been indicated by *Shimamura and Takayanagi* [1984]. In an electron collision with a polyatomic molecule at energies above the first threshold for emission, the interaction time between the electron and atom will be very short compared to the rotational or vibrational periods. In a close encounter with a sulfur atom in a sulfur-containing polyatomic molecule, the main force an electron will feel will be from the sulfur atom. The contribution of cascade is probably negligible in both the cases, S + e and SO_2 + e. In a recent paper by *Zatsarinny and Tayal* [2002], the authors have estimated the maximum cascade cross section to the emission cross section is about 10% from principal quantum number n = 5 states and another 10% for states with n > 5. The oscillator strengths normally scale as $1/n^3$, which means higher member contributions decrease rapidly. At 200 eV, electron-impact energy cross section for the atomic multiplet S I 1479 Å was determined by summing the measured cross sections for the features 31 and 32 of Table 1; this cross section was estimated to be 1.35×10^{-18} cm^2. We attempted here to estimate the emission cross sections as a function of electron-impact energy for S I 1479 Å from SO_2 by using the excitation data (for SO_2 + e → S I 1479 Å process) from an earlier publication by *Ajello et al.* [1992]. The measured cross section at 200 eV was used as a benchmark to obtain cross sections for the energy range 20–800 eV; they are presented in Table 6. A comparison of the emission cross sections of S I 1479 Å from SO_2 + e (see Table 5) with those of S + e [*Zatsarinny and Tayal*, 2002] is shown in Figure 11. As seen from the figure the cross sections in the case of SO_2 were always much smaller than those of atomic sulfur. However the correspondingly higher column densities of SO_2 can make up this deficiency found at Io [*Wong and Smyth*, 2000].

[33] We can proceed a step further by applying the analysis in a very simple optically thin model of two atmospheric layers to the Aug 1998 STIS observation analyzed by *Feaga et al.* [2002]. The two layers are an emission layer of SO_2 within the thermosphere and an absorbing layer comprised of the S-atoms inside the exosphere. We model the opacity at line center of a high-altitude absorption layer of S atoms, which are characterized by an exospheric temperature of about 1 eV. The exospheric

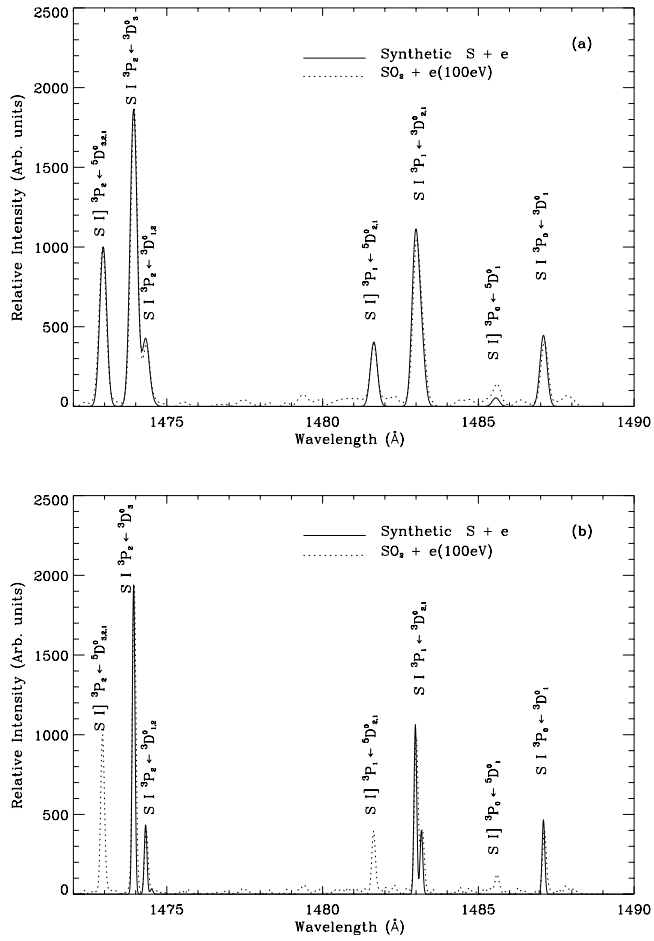

Figure 10. (a) A comparison of the fine structure intensities for the S I 1479 Å multiplet from electron impact on atomic sulfur (model) and SO2 (laboratory spectrum at 100 eV electron impact energy and resolution 95 mÅ was taken from Figure 4a and was subsequently convolved to 235 mÅ FWHM). (b) A comparison of the optically allowed fine structure intensities for the S I 1479 Å multiplet from electron impact on atomic sulfur (model) and SO_2 (laboratory spectrum at 100 eV electron impact energy and resolution 95 mÅ was taken from Figure 4a).

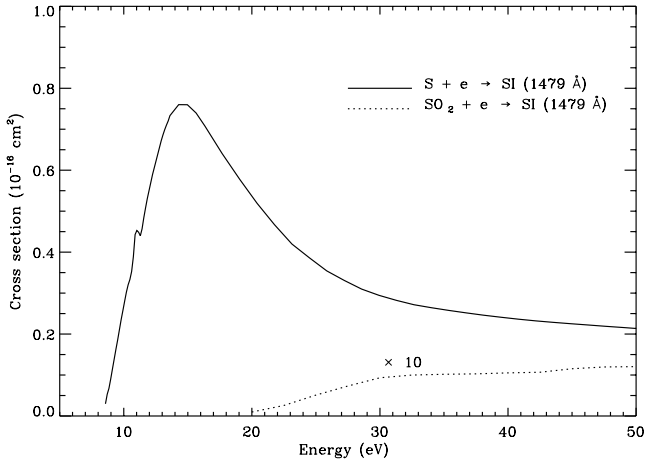

Figure 11. A comparison of emission cross sections for S I 1479 Å from SO_2 + e (present measurement) with those from the theoretically calculated cross sections for S + e by *Zatsarinny and Tayal* [2001, 2002]. The total cross sections for S + e, indicated by the solid line, was obtained by adding the calculated cross sections for the optically allowed transitions ($3s^2\ 3p^4\ ^3P \leftarrow 3s^2\ 3p^3\ 4s^3\ D^0$) [*Zatsarinny and Tayal*, 2002] and the optically forbidden transitions ($3s^2\ 3p^4\ ^3P \leftarrow 3s^2\ 3p^3\ 3d^5\ D^0$) [*Zatsarinny and Tayal*, 2001].

temperature is based on the release of fast sulfur atoms from dissociative excitation inside the thermosphere. A portion of the fast sulfur atoms will travel upwards to form the collisionless exosphere. A model-based column density of $\sim 1 \times 10^{13}$ cm^{-2} in the exosphere of S-atoms can attenuate the upward intensity of 1479 Å photons from the SO_2 emission layer located in the thermosphere, by about 50% to produce the same intensity as the observation. The model assumes that the Doppler line emission profile from the thermosphere is characterized by a nonthermal Doppler width of about 1 eV and that secondary emission is negligible. The results are shown in Figure 12 for the 100 eV spectrum (analysis with the 30 eV spectrum produces identical results as indicated in Figure 4b). In this model the temperature of the gas in the thermosphere is lower (~0.2 eV) [*Strobel et al.*, 1994] than that of the exosphere (1 eV). A small segment of the emission line near line center will also be absorbed by the cooler thermosphere gas distribution of sulfur atoms. The model results in Figure 12 for the process of e + SO_2 are nearly the same as the model plots of Feega et al. for the process e + S. Thus from a measurement at the STIS G140M resolution of the 1479 Å multiplet fine structure it is not possible to distinguish whether the primary emission source is S or SO_2. The model presented here is vastly oversimplified neglecting the following: (1) multiple scattering including photon entrapment, (2) absorption within the cooler thermosphere layer, (3) the kinetic energy distribution of S-atoms from dissociation of SO_2 into neutral ground state fragments which may

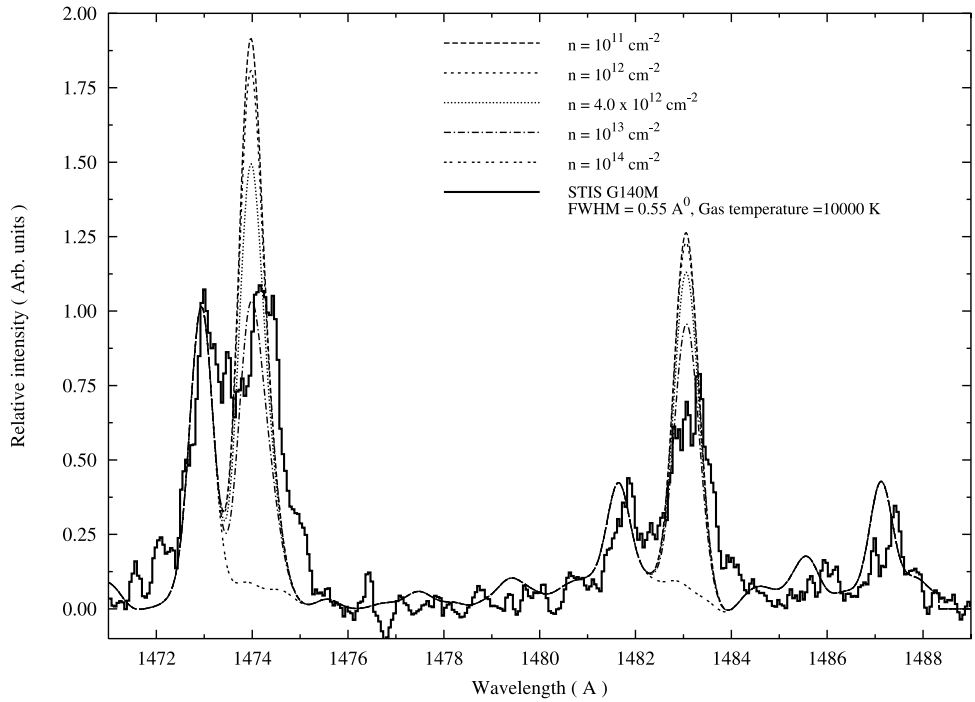

Figure 12. A model of the STIS G140M (resolution 0.6 Å) observation of August 1998 [*Feaga et al.*, 2002] for the 1479 Å fine structure based on a lower atmosphere emission source of SO_2 and transmission through an upper atmosphere layer of atomic S, producing self-absorption in the exosphere as explained in the text. The exosphere gas temperature was taken to be 10000 K. The model lines overlap in the vicinity of the forbidden transitions. The SO_2 laboratory spectrum at 100 eV electron impact energy and resolution 95 mÅ was taken (from Figure 4a) and was subsequently convolved to 0.55 Å FWHM.

be less than the fast sulfur excited atoms of this study, and (4) proper apportionment of absorption of 1479 Å photons by exospheric S-atoms having different temperatures. Column densities of S-atoms of $\sim 1 \times 10^{13}$ cm^{-2} in the exosphere are plausible from the detailed models of *Wong and Smyth* [2000] which indicate exobase column densities $>1 \times 10^{13}$ cm^{-2}. Perhaps the large extent of the Io corona to distances of 10–20 Io radii [*Wolven et al.*, 2001; *Roesler et al.*, 1999] may be partially explained by the release in the thermosphere of superthermal S-atoms in the dissociation processes involving SO_2. A model incorporating all these processes may be able to better treat the question of the principal emission source as being S or SO_2 or really a combination of the two target species. The development of this model is outside the scope of the present work.

[34] **Acknowledgments.** The research described in this text was carried out at the Jet Propulsion Laboratory, California Institute of Technology. The work was supported by the Air Force Office of Scientific Research (AFOSR), the Aeronomy Program of the National Science Foundation Program (grant ATM-9320589), and NASA Planetary Atmospheres, Astronomy/Astrophysics and Space Physics Program Offices. P. Vatti Palle acknowledges the support of National Research Council Resident Research Associateships. We have benefited from fruitful discussions with S. Tayal, D. Strobel, and W. Smyth. We thank M. McGrath for providing the HST GHRS spectrum and L. Feega for furnishing the August 1998 STIS spectrum of the 1479 Å multiplet.

[35] Arthur Richmond thanks William McConkey and Darrell Strobel for their assistance in evaluating this paper.

References

Ajello, J. M. (1970), Emission cross sections of N_2 in the vacuum ultraviolet by electron impact, *J. Chem. Phys.*, *53*, 1156–1165.

Ajello, J. M., et al. (1988), Simple ultraviolet calibration source with reference spectra and its use with the Galileo orbiter ultraviolet spectrometer, *Appl. Opt.*, *27*, 890–914.

Ajello, J. M., G. K. James, I. Kanik, and O. B. Franklin (1992a), The complete UV spectrum of SO2 by electron impact: 1. The vacuum ultraviolet spectrum, *J. Geophys. Res.*, *97*, 10,473–10,500.

Ajello, J. M., G. K. James, I. Kanik, and O. B. Franklin (1992b), The complete UV spectrum of SO_2 by electron impact: 2. The middle ultraviolet spectrum, *J. Geophys. Res.*, *97*, 1050–10,512.

Ajello, J. M., S. M. Ahmed, I. Kanik, and R. Multari (1995a), Kinetic energy distributions of H (2p) atoms from dissociative excitation of H_2, *Phys. Rev. Lett.*, *75*, 3261–3264.

Ajello, J. M., I. Kanik, S. M. Ahmed, and J. T. Clarke (1995b), Line profile of H Lyman-α from dissociative excitation of H_2 with application to Jupiter, *J. Geophys. Res.*, *100*, 26,411–26,420.

Ajello, J. M., S. M. Ahmed, and X. Liu (1996), Line profile of H Lyman-β from dissociative excitation of H_2, *Phys. Rev. A.*, *53*, 2303–2308.

Bhardwaj, A., and M. Michael (1999a), On the excitation of Io's atmosphere by the photo-electrons: Application of the analytical yield spectral model of SO_2, *Geophys. Res. Lett.*, *26*, 393–396.

Bhardwaj, A., and M. Michael (1999b), Monte Carlo model for electron degradation in SO_2 gas: Cross section, yield spectra and efficiencies, *J. Geophys. Res.*, *104*, 24,713–24,728.

Clarke, J. T., J. M. Ajello, J. Luhmann, and N. Schneider (1992), HST FOS spectra of Io passing into eclipse, *Bull. Astron. Soc.*, *24*, 936.

Clarke, J. T., J. M. Ajello, J. Luhmann, N. Schneider, and I. Kanik (1994), Hubble Space Telescope UV spectral observations of Io passing into eclipse, *J. Geophys. Res.*, *99*, 8387–8402.

Esposito, L., et al. (2003), Cassini ultraviolet imaging spectrograph investigation, *Space. Sci. Rev.*, in press.

Feaga, L. M., M. A. McGrath, and P. D. Feldman (2002), The abundance of atomic sulfur in the atmosphere of Io, *Astrophys. J.*, *570*, 439–446.

Feldman, P. D., F. D. Strobel, H. W. Moos, K. D. Retherford, B. C. Wolven, M. A. McGrath, F. L. Roesler, C. R. Woodward, R. J. Oliversen, and G. E. Ballester (2000), Lyman-α imaging of the SO_2 distribution on Io, *Geophys. Res. Lett.*, *27*, 787–790.

Frank, L. A., and W. R. Paterson (1999), Intense electron beams observed at Io with the Galileo spacecraft, *J. Geophys. Res.*, *104*, 28,657–28,669.

Frank, L. A., and W. R. Paterson (2000), Observations of plasma in the Io torus with the Galileo spacecraft, *J. Geophys. Res.*, *105*, 16,017–16,034.

Frank, L. A., and W. R. Paterson (2002), Plasmas observed with the Galileo spacecraft during its flyby over Io's northern polar region, *J. Geophys. Res.*, *107*(A8), 1220, doi:10.1029/2002JA009240.

Frank, L. A., W. R. Paterson, K. L. Akerson, V. M. Vasyliunas, F. V. Coroniti, and S. J. Bolton (1996), Plasma observations at Io with the Galileo spacecraft, *Science*, *274*, 394–395.

Geissler, P. E., A. C. McEwen, W. Ip, M. J. S. Belton, T. V. Johnson, W. H. Smyth, and A. P. Ingersoll (1999), Galileo imaging of atmospheric emissions from Io, *Science*, *285*, 870–874.

Hall, D. T., D. F. Strobel, P. D. Feldman, M. A. McGrath, and H. A. Weaver (1995), Detection of an oxygen atmosphere on Jupiter's moon Europa, *Nature*, *23*, 677–679.

Hall, D. T., P. D. Feldman, M. A. McGrath, and D. F. Strobel (1998), The far ultraviolet oxygen airglow of Europa and Ganymede, *Astrophys. J.*, *499*, 475–481.

Jackman, C. H., R. H. Garvey, and A. E. S. Green (1977), Electron impact on atmospheric gases: 1. Updated cross sections, *J. Geophys. Res.*, *82*, 5081–5090.

Kanik, I., C. Noren, O. P. Makarov, P. Vattipalle, J. M. Ajello, and D. E. Shemansky (2003), Electron impact dissociative excitation of O_2: 2. Absolute emission cross sections of the OI (130.4 nm) and OI (135.6 nm) lines, *J. Geophys. Res.*, *108*(E11), 5126, doi:10.1029/2000JE001423.

Liu, X., S. M. Ahmed, R. A. Multari, G. K. James, and J. M. Ajello (1995), High resolution electron impact study of the far ultraviolet emission spectrum of molecular hydrogen, *Astrophys J. Suppl. Ser.*, *101*, 375–399.

Makarov, O. P., I. Kanik, and J. M. Ajello (2003), Electron impact dissociative excitation of O_2: 1. Kinetic energy distributions of fast oxygen atoms, *J. Geophys. Res.*, *108*(E11), 5125, doi:10.1029/2000JE001422.

Michael, M., and A. Bhardwaj (2000), FUV emissions on Io: Role of Galileo-observed field-aligned energetic electrons, *Geophys. Res. Lett.*, *27*, 3139–3140.

Ogawa, T., and H. Higo (1979), Analysis of the translational energy of H* produced in e − H_2 collisions, *Chem. Phys. Lett.*, *65*, 610–612.

Ogawa, T., and H. Higo (1980), Translational energy distribution and production of excited hydrogen atoms produced by controlled electron impact of H_2, *Chem. Phys.*, *52*, 55–64.

Ogawa, T., S. Ihara, and K. Nakashima (1992), Fano plots for the slow and fast groups of hydrogen atoms produced in e − H_2 collisions, *Chem. Phys.*, *161*, 509–513.

Oliversen, J. R., F. Scherb, W. H. Smyth, M. E. Freed, R. C. Woodward Jr., M. L. Marconi, K. D. Retherford, O. L. Lupie, and J. P. Morgenthaler (2001), Sunlit IO atmospheric [O I] 6320 Å emission and plasma torus, *J. Geophys. Res.*, *106*, 26,183–26,194.

Press, W. H., B. P. Flannery, S. A. Teukolsky, W. T. Wettering (1986), *Numerical Recipes*, 818 pp., Cambridge Univ. Press, New York.

Retherford, K. D., H. W. Moos, D. F. Strobel, and B. C. Wolven (2000), IO's equatorial spots-Morphology of neutral UV emissions, *J. Geophys. Res.*, *105*, 27,157–27,165.

Roesler, F. L., H. W. Moos, R. J. Oliversen, R. C. Woodward Jr., W. H. Smyth, P. D. Feldman, and D. F. Strobel (1999), Far ultraviolet imaging spectroscopy of IO′s atmosphere with HST/STIS, *Science*, *283*, 353–357.

Shimamura, I., and K. Takayanagi (1984), *Electron–Molecule Collisions*, Plenum, New York.

Spencer, J. R., and N. M. Schneider (1996), Io on the eve of Galileo mission, *Annu. Rev. Earth Planet. Sci.*, *24*, 125–190.

Strobel, D. F., X. Zhu, and M. E. Summers (1994), On the vertical thermal structure of Io's atmosphere, *Icarus*, *11*, 18–30.

Van Brunt, R. J., and R. N. Zare (1968), Polarization of atomic fluorescence excited by molecular dissociation, *J. Chem. Phys.*, *48*, 4304–4308.

Wolven, B. C., H. W. Moos, K. D. Retherford, P. D. Feldman, and D. F. Strobel (2001), Emission profiles of neutral oxygen and sulfur in Io's exospheric corona, *J. Geophys. Res.*, *106*, 26,155–26,182.

Wong, M. C., and W. H. Smyth (2000), Model calculations for Io's atmosphere at eastern and western elongations, *Icarus*, *146*, 60–74.

Zatsarinny, O., and S. S. Tayal (2001), Low-energy electron collisions with atomic sulfur: R-matrix calculation with non-orthogonal orbitals, *J. Phys., B. At. Mol. Opt. Phys.*, *34*, 3383–3400.

Zatsarinny, O., and S. S. Tayal (2002), Electron impact collision strengths and rates for neutral sulfur using the B-Spline R-matrix approach, *J. Phys., B. At. Mol. Opt. Phys.*, *35*, 2493–2503.

J. Ajello and P. Vatti Palle, Jet Propulsion Laboratory, California Institute of Technology, Pasadena, CA 91109, USA. (jajello@jpl.nasa.gov)

A. Bhardwaj, Space Physics Laboratory,Vikram Sarabhai Space Centre, Trivandrum 690522, India.